Evolution of orthorhombic domain structures during the tetragonal-to-orthorhombic phase transition in the layered perovskite $Sr_{2-x}La_xMnO_4$

Wataru Norimatsu and Yasumasa Koyama
Department of Materials Science and Engineering, and Kagami Memorial Laboratory for Materials Science and Technology, Waseda University, Shinjuku-ku, Tokyo 169, Japan
(Received 18 May 2006; published 15 August 2006)

When Sr^{2+} ions in Sr_2MnO_4 containing only Mn^{4+} ions were partially replaced by La^{3+}, a new phase having orthorhombic symmetry appeared around an La content of $x=0.15$ between the tetragonal $I4/mmm$ (T) phase and the charge and orbital ordered (COO) phase, accompanying the introduction of Mn^{3+} ions. Our *in situ* observation using a transmission electron microscope revealed that the orthorhombic (O) phase could be identified as an orbital ordered state without charge ordering, and that its microstructure is characterized by an alternating array of two banded-shape variants with different orthorhombicities, O_I and O_{II}. It was also found that the T-to-O phase transition exhibited a unique evolution of domain structures, which resulted in the above-mentioned banded microstructure. In particular, the domain-structure evolution consisted of three steps: the appearance of the $(T+O_I)$ and then the (O_I+O_{II}) coexisting states, followed by the annihilation of the interface between the O_I and O_{II} variants. The evidence suggests that this unique pattern of evolution is due to coupling between the short-wavelength Jahn-Teller (JT) distortion, associated with the Mn^{3+} ion, and the long-wavelength O distortion.

DOI: 10.1103/PhysRevB.74.085113 PACS number(s): 75.47.Lx, 68.18.Jk, 71.38.−k, 68.37.Lp

I. INTRODUCTION

Among the family of strongly correlated electron compounds, manganites with a simple perovskite structure exhibit a variety of interesting phenomena, including colossal magnetoresistance (CMR).[1–5] An important characteristic of these materials is the coexistence of two competing phases, with nanometer and micrometer scales, in the vicinity of a phase boundary between them. The CMR effect is, in fact, associated with a spatially inhomogeneous state with mesoscopic length scale near a boundary between the ferromagnetic metallic (FM) and antiferromagnetic charge and orbital ordered (COO) phases.[6–11] It was pointed out that the appearance of the inhomogeneous state originates from the random interaction produced by, for instance, quenched disorder.[10,11] In the COO phase, on the other hand, there are incommensurate COO (ICOO) structures, including higher-order commensurate COO (CCOO) structures, whose modulation modes involve an array of Mn^{3+} stripes and a Jahn-Teller (JT) distortion. As for the ICOO and higher-order CCOO structures, their origins have been explained as being due to competing interactions, as was pointed out in the axial next nearest neighbor Ising (ANNNI) model.[12,13] Because of the importance of the JT distortion in the COO phase, there should be competition between the ferrodistortive (FD) and antiferrodistortive (AFD) interactions; that is, the interactions between two neighboring JT clusters.[6–9,14] The presence of the ICOO structures and the AFD state has also been reported in the layered perovskite $Sr_{2-x}La_xMnO_4$ with the K_2NiF_4-type structure, which is dealt with in this study.

Sr_2MnO_4 containing only Mn^{4+} ions is an insulator with an electronic configuration of t_{2g}^3.[15–19] When Sr^{2+} ions are partially replaced by La^{3+} ions in $Sr_{2-x}La_xMnO_4$, Mn^{3+} ions are introduced into the system by doping e_g electrons. According to the previous work of Larochelle *et al.*,[18,19] the ICOO structures, including higher-order CCOO structures, exists in the region $0.3<x<0.5$ and the AFD state appears in $x=0.5$ as the CCOO structure with a periodicity of $4d_{110}$, where d_{110} is the interplanar distance of the (110) plane. The important feature of the COO phase is that the inverse ζ of the periodicity shows a linear relation with the La content x as $\zeta=x/2$. In other words, the inverse of an average distance between two neighboring Mn^{3+} stripes increases linearly with increasing x. In addition to the COO phase, the orthorhombic (O) phase with space group of *Immm* has been reported around $x=0.2$ in layered manganites such as $Sr_{2-x}Nd_xMnO_4$.[20,21]

The appearance of the ICOO structures in $Sr_{2-x}La_xMnO_4$ presumably arises from the competition between the FD and AFD interactions, just as in other manganites. This suggests that the ICOO state, including higher-order CCOO structures, in the COO phase must exist between the FD and AFD states in a phase diagram. It is understood that the FD state is stabilized by an indirect interaction between JT clusters via a phonon field, while a direct interaction results in the AFD state. Since the ICOO and AFD states were respectively reported in the region $0.3<x<0.5$ and $x=0.5$ in $Sr_{2-x}La_xMnO_4$, the FD state would be present at smaller La contents, presumably around $x=0.2$. In other words, the O phase, reported in $Sr_{2-x}Nd_xMnO_4$ around $x=0.2$, might be identified as the FD state.[20–22]

To probe these issues, we have investigated the crystallographic features of $Sr_{2-x}La_xMnO_4$ with $0\leqslant x\leqslant 0.5$ by transmission electron microscopy. As a result, the O phase was actually found around $x=0.15$ between the tetragonal $I4/mmm$ (T) and ICOO states. There is also an ICOO state in the $0.2\leqslant x\leqslant 0.3$ region as well as for $0.3<x<0.5$. The linear relation between ζ and x was confirmed to be satisfied over the whole COO region of $0.2\leqslant x\leqslant 0.5$. Furthermore, we found both an interesting domain structure in the O phase to be the FD state and a unique evolution of the domain structure in the T-to-O phase transition around $x=0.15$. In

this paper, we then describe the details of the experimental data on the layered perovskite $Sr_{2-x}La_xMnO_4$, which were obtained mainly by low-temperature *in situ* observation using a transmission electron microscope (TEM).

II. EXPERIMENTAL PROCEDURE

$Sr_{2-x}La_xMnO_4$ samples with $0 \leqslant x \leqslant 0.5$ were prepared by the coprecipitation technique using citric acid. We did not use a solid-state-reaction after discovering that samples made by this method contained micron-scale inhomogeneities in chemical composition. The detailed sample preparation procedure involved calcining initial sample powders obtained by coprecipitation from $SrCO_3$, La_2O_3, and $MnCO_3$ powders at 1123 K for 12 h. After the powders were pressed into pellets, they were sintered at 1773 K for 24 h in an O_2 atmosphere. The crystallographic features of the samples obtained in this way were examined by x-ray powder diffraction and transmission electron microscopy. The x-ray diffraction experiments were conducted to examine the change in average structures in the temperature range between room temperature and 10 K. The x-ray apparatus used in this study was a Rigaku-RINT-TTR with a low-temperature stage, operated at 50 kV and 300 mA. Both the domain structure and the domain-structure evolution in the O phase were examined by low-temperature *in-situ* observation using a JEM-3010 type transmission electron microscope equipped with a liquid He-cooled holder. Note that the lowest temperature obtained in the TEM studies was 12 K. Thin specimens for transmission electron microscopy observation were prepared by the Ar-ion thinning method.

III. EXPERIMENTAL RESULTS

Figure 1 shows the phase diagram on the La-poor side, determined on the basis of our experimental data obtained by x-ray powder diffraction and transmission electron microscopy. A schematic diagram of the FD and AFD states is also depicted. The FD state exists in $0.10 \leqslant x \leqslant 0.20$ region, the ICOO state for $0.20 \leqslant x < 0.5$, and the AFD state at $x=0.5$. At that point, the FD and AFD states are detected as, respectively, the O phase and the CCOO structure with a $4d_{110}$ periodicity in the COO phase. As is shown in the inset, the inverse ζ of the periodicity n satisfies a linear relation with respect to the La content x in the COO phase. It is known that the AFD state has a $2d_{110}$ periodicity of the array of Mn^{3+} stripes as charge ordering and a $4d_{110}$ periodicity for the JT distortion corresponding to the alternate array of the $(3x^2-r^2)$ and $(3y^2-r^2)$ orbitals. On the other hand, our experimental data indicate that the FD state is a charge disordered (CD) state characterized only by the $(3x^2-r^2)$ or $(3y^2-r^2)$ orbital. In other words, the ferro-orbital FD state results in the orthorhombic distortion. The magnitude of orthorhombic distortion should depend on the degree of orbital ordering. The experimental evidence for this distinct characteristic of the O phase will be described below.

Dark field images exhibiting the microstructures of the *T*, FD, and ICOO states at 15 K are shown in Fig. 2, together with their 200 profiles in x-ray powder diffraction patterns.

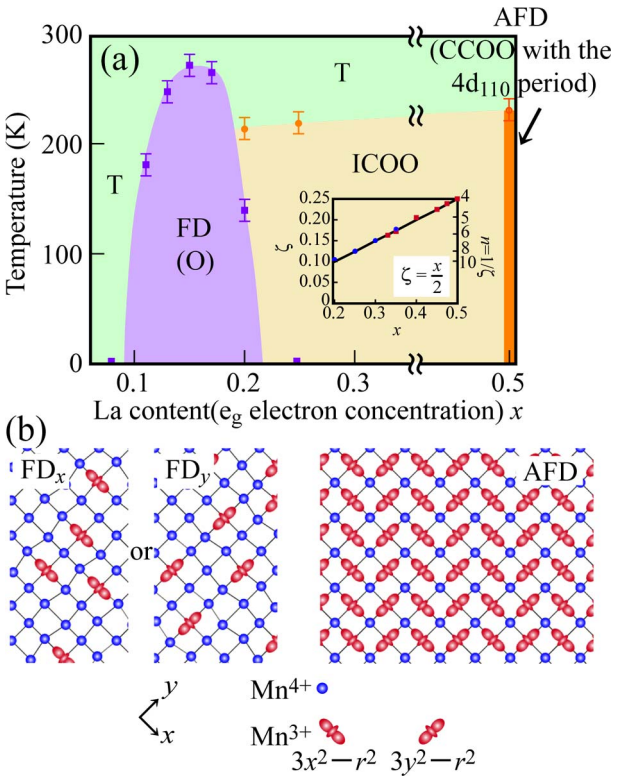

FIG. 1. (Color online) (a) La-poor portion of the phase diagram for $Sr_{2-x}La_xMnO_4$, which was obtained on the basis of our experimental data, and (b) schematic diagrams indicating the ferrodistortive (FD) and antiferrodistortive (AFD) states. Note that the La content in the phase diagram corresponds to the e_g electron concentration; that is, the Mn^{3+} content. In the phase diagram, there exist the high-symmetry tetragonal (*T*) state for $x \leqslant 0.10$, the FD state for $0.10 \leqslant x \leqslant 0.20$, the incommensurate charge and orbital ordered (ICOO) state for $0.20 \leqslant x < 0.50$, and the AFD state for $x=0.5$. The FD_x and FD_y variants in the ferro-orbital FD state are characterized by the $(3x^2-r^2)$ and $(3y^2-r^2)$ orbital orderings for the Mn^{3+} ions.

The images of these states were actually obtained from the $x=0.08$, 0.15, and 0.23 samples by using the respective 200, 660, and 200 and surrounding satellite reflections. In the *T* state exhibiting a single 200 peak in the powder pattern, first we see the tweed pattern in the image. The tweed pattern in this case is ascribed to a strain field produced by the presence of local O regions with lower symmetry in the *T* matrix. That is, there is a precursor state of the *T*-to-O phase transition even at $x=0.08$. Because of the orthorhombic symmetry in the O phase, the microstructure of the O phase as the FD state is a banded structure, and the 200 peak is split into two in its XRD profile. It seems that the banded structure can be identified as a twin structure consisting of two O variants with the same orthorhombicity b/a, resulting from the *T*-to-O transition. But, the present study indicated that the banded structure in the O state was characterized by an alternate array of two kinds of O bands with different b/a values, as will be clarified later. In the image of the $x=0.23$ sample in the ICOO state, fringes with a periodicity of about $8.7d_{110}$ are observed along the [110] direction, corresponding to the periodicity of the JT distortion as a response of the lattice system to the $(3x^2-r^2)/(3y^2-r^2)$ orbital ordering.

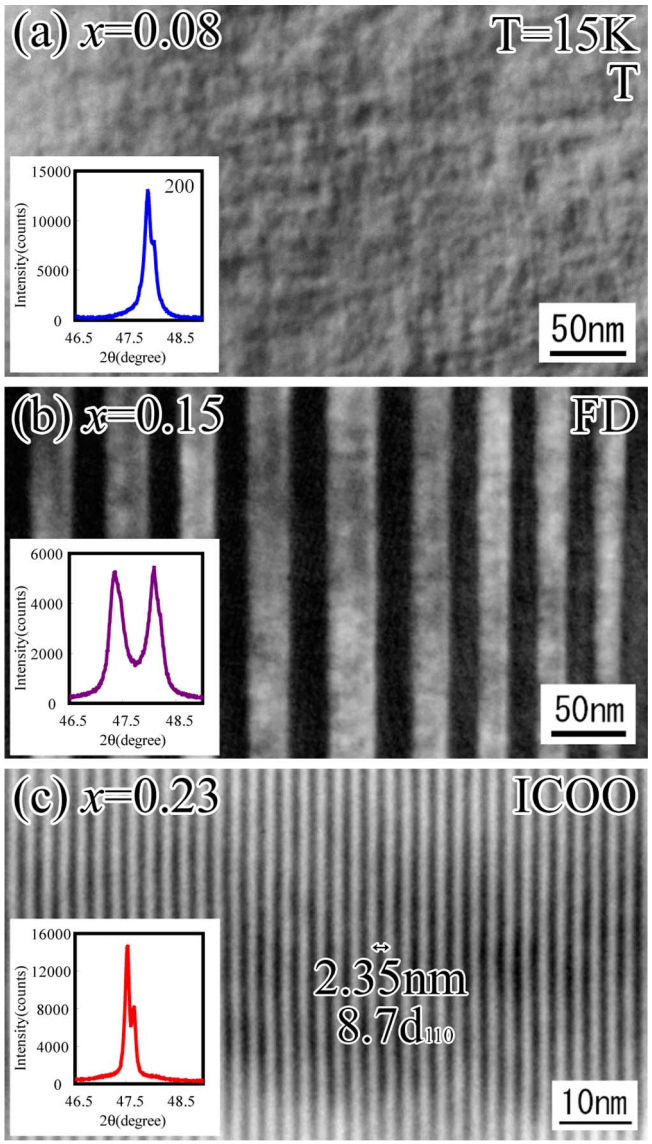

FIG. 2. (Color online) Dark field images showing the microstructures of the T, FD, and ICOO states at 15 K, together with their corresponding 200 reflections in x-ray powder diffraction profiles. The T, FD, and ICOO images were taken from the x= (a) 0.08, (b) 0.15, and (c) 0.23 samples, respectively. The electron incidence of these images was parallel to the $[001]_T$ direction, where the subscript T denotes the T state.

Note that, because of their weak intensities, the superlattice peaks produced by the modulation from the JT distortion are not detected in the powder pattern.

Before describing the unique evolution of the domain structure in the T-to-O phase transition, we report the characteristic of the O phase as the FD state, which was obtained by using the ICOO-to-O transition. Figure 3 shows the change in electron diffraction patterns in the vicinity of the 660 position in reciprocal space during the ICOO-to-O transition of the x=0.20 sample, together with intensity profiles along the $[1\bar{1}0]$ direction through the 660 position. The pattern and profile at 190 K, where the sample is in the ICOO state exhibit the 660 fundamental reflection due to the T

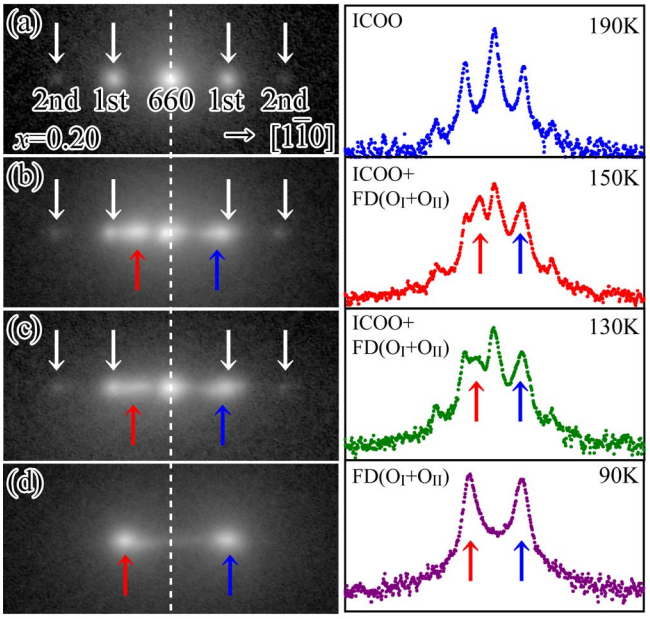

FIG. 3. (Color online) Change in electron diffraction patterns around the 660 position in reciprocal space during the ICOO-to-O transition, together with their intensity profiles along the $[1\bar{1}0]_T$ direction through it. The electron incidence of these patterns is parallel to the $[001]_T$ direction. The patterns in (a), (b), (c), and (d) were taken, respectively, from the x=0.20 sample at 190 K (ICOO), 150 K (ICOO+FD), 130 K (ICOO+FD), and 90 K (FD). In the pattern, a white broken line is a visual guide for the 660 position in reciprocal space. The reflections and peaks due to the O_I and O_{II} variants in the O state are denoted by the blue and red arrows.

state, and the first satellite reflections at $\vec{q}=[1/10,\overline{1/10},0]$, and the second reflections at $\vec{q}=[1/5,\overline{1/5},0]$. The satellite reflections originate from the modulation for the JT distortion, and the presence of the second harmonics is direct evidence that the modulation is sinusoidal. The periodicity of the modulation is determined to be $10d_{110}$ from the location of the first satellite reflection, which satisfies the linear relation of $\zeta=x/2$ for x=0.20. When the temperature is lowered to 150 K, two reflections indicated by the red and blue arrows appear in the pattern, in addition to the 660 fundamental and satellite reflections. The crucial feature of the new reflections is that their locations are asymmetric with respect to the 660 fundamental reflection. This implies that two O variants with b/a=1.016 and 1.009 are nucleated in the ICOO state. Note that these b/a values were calculated from angles given by the shifts of intensity peaks indicated by the blue and red arrows with respect to the fundamental 660 reflection. On further cooling, the reflection with the small b/a value is shifted to the larger value, while the location of the latter remains almost unchanged, as is shown in the pattern and profile at 130 K. Finally, at 90 K, the 660 fundamental and satellite reflections disappear and only two O reflections exist, indicating the existence of a single O phase. The notable feature of the O phase is that the locations of these two reflections are still asymmetric. The import of all these observations is that the domain structure in the O phase as the FD state consists of two O variants with different b/a

values, and that the ICOO-to-O phase transition occurs via the two-phase state.

Dark field images of the $x=0.20$ sample in the two-phase state were taken to examine the positional relation between the ICOO and two O variants. Figure 4 shows three dark field images at 190 K, 130 K, and 90 K, taken using the 200 fundamental and surrounding reflections. When the $x=0.20$ sample was cooled from the single ICOO state, fine bands indicating a charge disordered (CD) region appeared locally along the fringes representing the modulation in the ICOO state, indicated by the blue arrows in the image at 190 K.[23] This CD band is here called the CD_I region. The image at 130 K also indicates that these CD_I regions develop with decreasing temperature, and that the microstructure is characterized by the alternate array of the ICOO and CD_I bands. In addition, an interesting feature is that new fine CD bands, labeled as the CD_{II} region, are also nucleated along the fringes in the interior of the ICOO bands, shown by the red arrows. Dark field images not shown here, taken using the red and blue reflections in the 130 K pattern of Fig. 3, confirm that the CD_I and CD_{II} bands have different b/a values. In other words, the $x=0.20$ sample at 130 K consists of the ICOO state and two O variants. On subsequent cooling, the banded structure characterizing the O phase as the FD state is finally formed by the annihilation of the ICOO regions, as is seen in the image at 90 K. A series of these images clearly show that the microstructure of the FD state consists of two O variants with different b/a values, and that the O distortion of the FD state reflects the local distortion of the ICOO state; that is, the JT distortion.

As for the ICOO-to-O transition shown in Figs. 3 and 4, the following thing should be remarked. When the specimen was cooled down from the ICOO state, the transition occurred in slightly higher temperature in thicker areas. That is, the alternating array of the O_I and O_{II} bands were already formed even at 130 K in such areas. In Fig. 4(b), the specimen thickness in the left side is slightly larger than that in the right side, and an O_{II} variant developed from the CD_{II} region can actually be detected in the left side, as indicated by the double arrow. Because the diffraction pattern was taken from a wide region of about 1 μm, the same intensities of the peaks between 150 K and 90 K, marked by the blue and red arrows in Fig. 3, reflects the presence of the alternating array of the O_I and O_{II} bands in thicker areas. In other words, a transition temperature of the ICOO-to-O transition seems to be very sensitive to a specimen thickness, which should be associated with the relaxation of a strain field produced by the transition.

As the above-mentioned experimental data clarify the distinct characteristic of the FD state, we here focus on the crystallographic features of the T-to-O phase transition occurring around $x=0.15$. We first describe the detailed change in the b/a values of two O variants during the transition. The change in the b/a values for the $x=0.15$ sample is shown in Fig. 5, together with corresponding electron diffraction patterns in the vicinity of the 660 position. When the temperature is lowered from the T phase, first the value of just the variant O_I deviates from zero at $T_1 \approx 270$ K, while the other O_{II} variant has a nonzero value below $T_2 \approx 240$ K. Hence, the $(T+O_I)$ two-phase state characterized by only one O

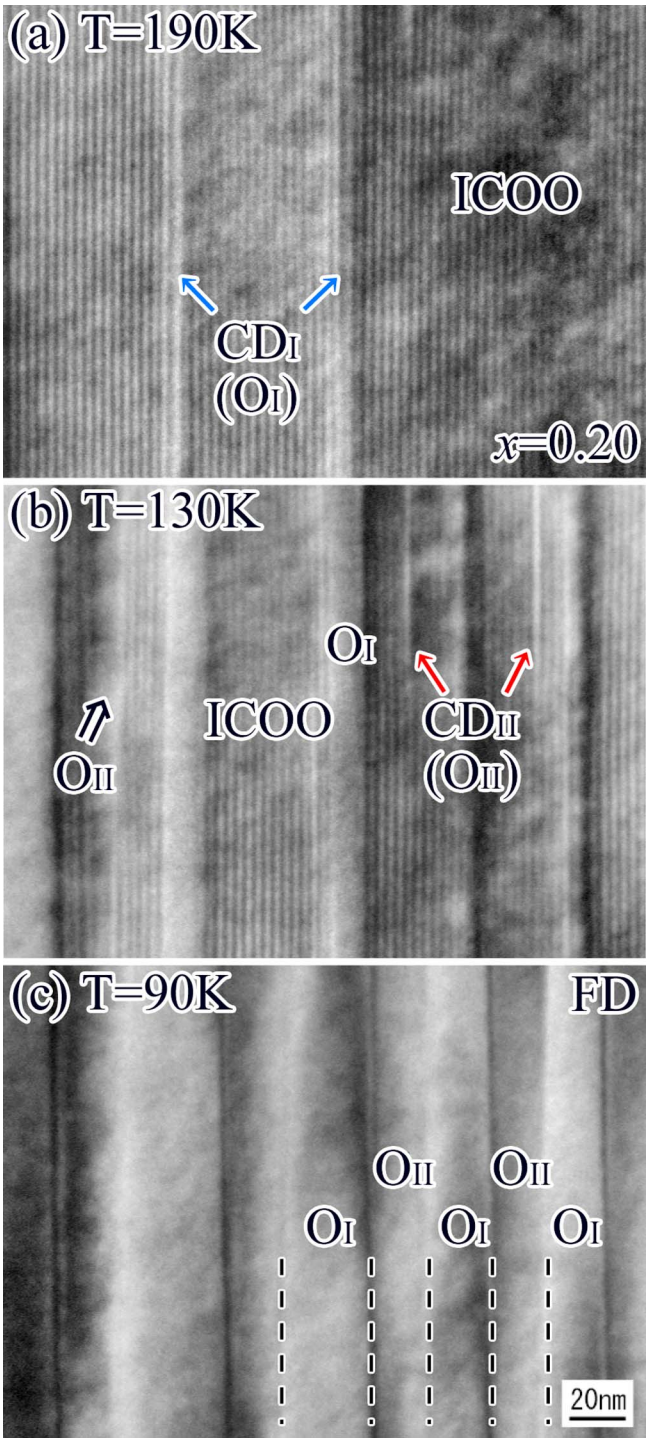

FIG. 4. (Color online) A series of dark field images showing the change in the microstructures during the ICOO-to-O transition. The images were taken from the $x=0.20$ sample at 190 K (ICOO), 130 K (ICOO+O_I), and 90 K (O_I+O_{II}), using the 200 fundamental and its satellite reflections. Two kinds of very thin charge-disordered regions, CD_I (O_I) and CD_{II} (O_{II}), are seen, as is indicated by the blue and red arrows.

variant exists in the temperature range $240\ \text{K} < T < 270\ \text{K}$. Further cooling then leads to an increase in the b/a values of the O_I and O_{II} variants, but these values never become equal even at a temprature as low as 12 K. Apparently, the

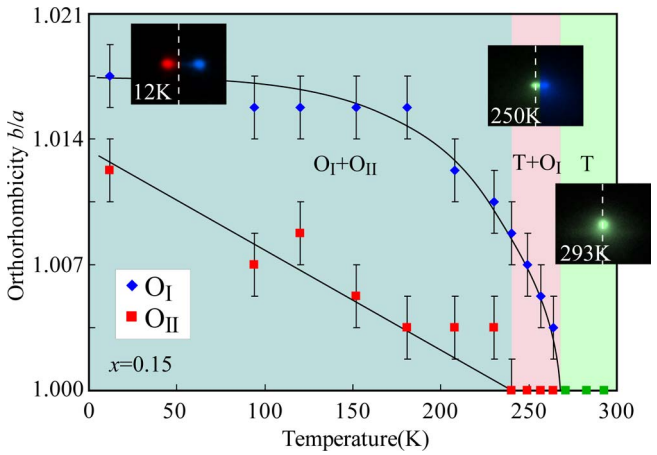

FIG. 5. (Color online) Variation of the b/a values of the O_I and O_{II} variants during the T-to-O phase transition in the $x=0.15$ sample. Parts of the electron diffraction patterns at 293 K (T), 250 K ($T+O_I$), and 12 K (O_I+O_{II}) are also shown in the insets. In each pattern, the white dashed line is a visual guide for the 660 position, and the green, blue, and red reflections are due, respectively, to the T phase, and the O_I and O_{II} variants. The b/a values of the O_I and O_{II} variants plotted here were determined from the locations of the O_I and O_{II} reflections at each temperature.

$x=0.15$ sample below T_2 is in a state consisting of two O variants with different b/a values, just as in the case of the $x=0.20$ sample. It is also understood that the difference in the b/a values for two O variants comes from the fact that the temperature T_2 for the appearance of the O_{II} variant is lower than T_1 for the O_I variant.

The evolution of the domain structure during the T-to-O phase transition, corresponding to the change in the b/a values shown in Fig. 5, was examined by taking the series of dark field images of the $x=0.15$ sample shown in Fig. 6, using the 660 reflections of the O_I and O_{II} variants. The images in the left and right sides of the figure were, respectively, taken using the reflections of the T phase or the O_{II} variant, and the O_I variant. In the images at 280 K in the T phase, the tweed pattern is seen in (a). It is obvious that the tweed pattern is an indication of the precursor state for the T-to-O transition, as was described for the $x=0.08$ sample in Fig. 2. That is, local O regions are involved in the T matrix.

When the temperature is lowered from that where the T phase exists, the image (b′) at 250 K in the $(T+O_I)$ two-phase state shows the appearance of the O_I variant having the thin banded shape. The tweed structure reflecting the average T symmetry is still observed in the bright-contrast bands of the image (b). Then, the $(T+O_I)\rightarrow O$ change takes place on subsequent cooling to around 240 K. At 160 K in the O phase, we then see the thin bands in both the (c) and (c′) images. This implies that the O_{II} variant is converted from the T bands exhibiting the tweed pattern, and that the microstructure at 160 K consists of an alternating array of the O_I and O_{II} bands. The major features of the microstructure are that the interface of the banded structure is basically parallel to the (110) plane, and that the average distance between two neighboring O_I bands is about 10 nm. On further cooling in the O phase, some thinner O_I and O_{II} bands are annihilated, as is seen in the images at 90 K, (d) and (d′). As a result of the annihilation, the average distance of the O_I bands becomes longer and is estimated to be about 50 nm. Note that the O_I and O_{II} variants at 90 K have the values of $b/a=1.016$ and 1.005, respectively. These results show that the evolution of the domain structure in the O phase occurs in three steps: the formation of two kinds of the banded structures, $T+O_I$ and O_I+O_{II}, and the subsequent annihilation of some thinner O_I and O_{II} bands. It seems that this unusual pattern of evolution has some similarity to that of chemical composition in a spinodal decomposition.[24,25]

IV. DISCUSSION

Both our experimental XRD and TEM data on the layered perovskite $Sr_{2-x}La_xMnO_4$, revealed that the O phase exists in the $0.10\leqslant x\leqslant 0.20$ composition region and is characterized by the CD state with the O distortion. Because the O distortion directly reflects the local symmetry of the COO state, the JT distortion, the O phase without charge ordering is identified as the FD state having the $(3x^2-r^2)$ or $(3y^2-r^2)$ orbital ordering. Figure 7 shows a schematic diagram for the appearance of the FD state in the ICOO matrix on the basis of the dark field image at 90 K in Fig. 4. The nucleation of the local FD state can easily occur by the melting of a one-dimensional array of e_g electrons in a Mn^{3+} stripe. The important point is that orbital ordering remains unchanged after the melting of charge ordering. This implies that the instability of a Mn^{3+} stripe in the ICOO state should strongly depend on the concentration of e_g electrons.

Based on the characteristic of the FD state just mentioned, the T-to-O phase transition characterized by the appearance of orbital ordering accompanies the introduction of both the JT and O distortions. Hence, the coupling between the JT and O distortions may be responsible for the unique behavior of the phase transition, as was pointed out by Ahn and coworkers.[6–9] Our observation have added to the understanding of this transition by tracing the interesting evolution of the O variants during the transition. Figure 8 depicts a one-dimensional schematic diagram indicating the evolution of the domain structures during the T-to-O phase transition. The upper and lower sides of the vertical axis in this diagram represent the b/a values of the O_I and O_{II} variants, shown previously in Fig. 5. The b/a value in the T phase, shown in Fig. 7(a), first has an average value, over the whole position, of zero, although the tweed pattern suggesting the presence of local O regions was observed in the dark field image. In the $(T+O_I)$ two-phase state, which was then obtained by cooling from the T phase, the O_I regions are pseudoperiodically arranged at an average interval of about 10 nm along the [110] direction in the T matrix. When the temperature is further lowered, the T region is changed into the O_{II} region, together with the widening of the O_I regions. Finally, the width of the O_I and O_{II} regions becomes larger through the annihilation of some thinner regions. With respect to Fig. 8, the T-to-O phase transition is characterized by both the spatial modulation of the O distortion and the subsequent annihilation of interfaces between the O_I and O_{II} variants, which are produced by the development of the b/a values. In par-

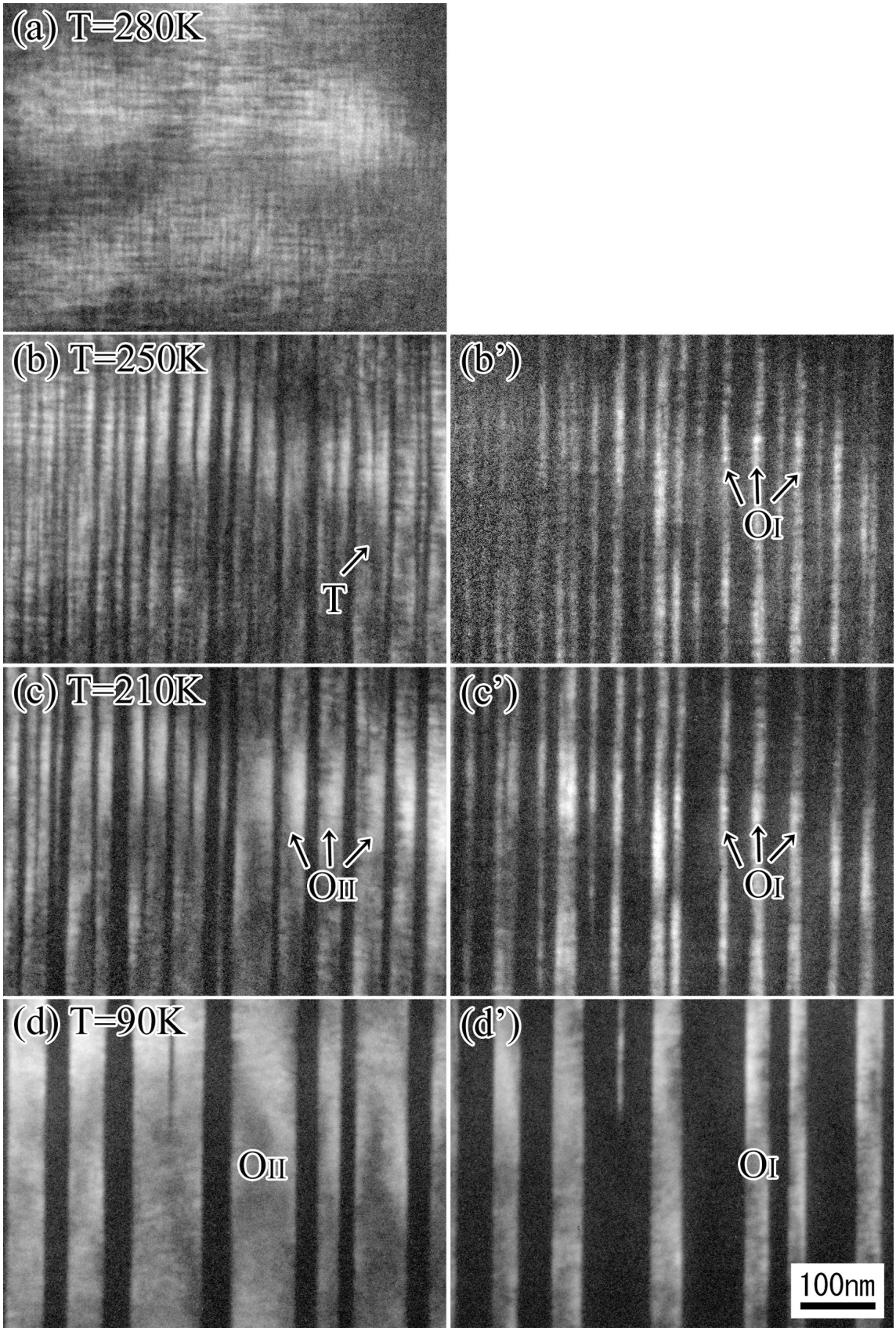

FIG. 6. A series of dark field images showing the domain-structure change during the T-to-O phase transition in the $x=0.15$ sample. The images in (a), (b) and (b′), (c) and (c′), and (d) and (d′) were taken, respectively, at 280 K (T), 250 K ($T+O_I$), 210 K (O_I+O_{II}), and 90 K (O_I+O_{II}). The electron incidence of all images is parallel to the [001] direction.

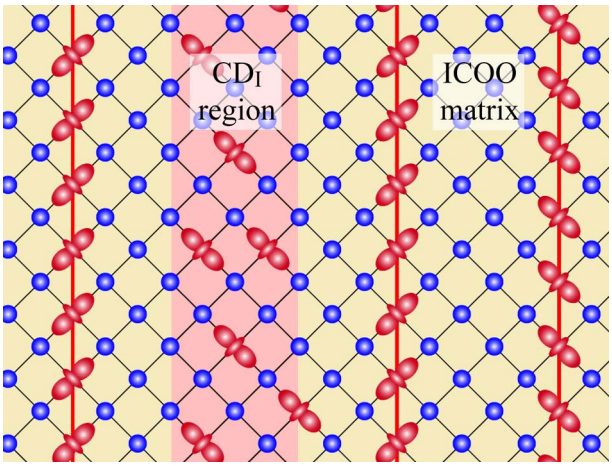

FIG. 7. (Color online) Schematic diagram showing the nucleation of a fine CD_I region in the ICOO matrix. The CD_I region indicated by the red area has orthorhombic symmetry, reflecting the $(3x^2-r^2)$-type orbital ordering. The appearance of the CD_I region is directly associated with the melting of a one-dimensional array of e_g electrons in the Mn^{3+} stripe.

ticular, there are two types of the modulation modes, $T+O_I$ and O_I+O_{II}, for this strain modulation. As far as we know, this domain-structure evolution is probably the first observed in condensed matter.

The intrinsic order parameter of the T-to-O phase transition is obviously the orbital ordering of the Mn^{3+} ions. The $(3x^2-r^2)$- and $(3y^2-r^2)$-type orderings result in the FD_x and FD_y states depicted in Fig. 1. The JT distortion should be a structural order parameter as a response of the lattice system

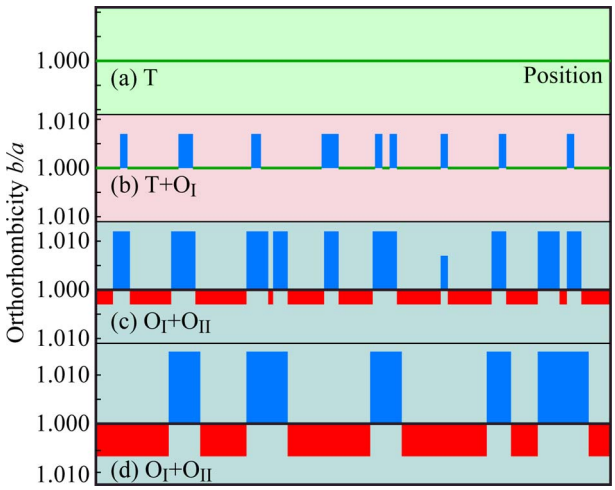

FIG. 8. (Color online) One-dimensional schematic diagram showing the domain-structure evolution during the T-to-O phase transition. In the diagram, the b/a values of the O_I variant at 250 K in Fig. 5, and the O_I and O_{II} variants at 210 K and 92 K are used, respectively, as those in (b) $(T+O_I)$, (c) (O_I+O_{II}), and (d) (O_I+O_{II}). When the temperature is lowered from that where the T phase exists, the banded (O_I+O_{II}) microstructure in the O phase is produced via the banded $(T+O_I)$ microstructure. In addition, coarsening of the O_I and O_{II} bands occurs at lower temperatures in the O phase by means of the annihilation of some thin bands.

to orbital ordering via the strong electron-lattice coupling. Because the JT distortion is also coupled to the O distortion, this coupling is presumably one of the possible origins for the unique evolution of the domain structures during this transition. Recently, Ahn and coworkers pointed out that the inhomogeneity seen in manganites could be explained as being due to the coupling between the short- and long-wavelength distortions.[6–9] In the case of the O phase in $Sr_{2-x}La_xMnO_4$, the short- and long-wavelength distortions are, respectively, identified as the JT and O distortions. Based on this correspondence, our experimental data seem to be entirely consistent with their calculated results. In particular, in addition to accounting for the appearance of the tweed pattern, the $(T+O_I)$ two-phase state is predicted as the alternating array of the undistorted and distorted regions in the case that their proposed energy landscape has a deep local minimum with respect to the short-wavelength distortion. It should be remarked at this point that their calculation dealt with the situation where the sample is kept at a certain temperature. In our study, the annihilation of the O_I and O_{II} bands could actually occur in such a situation, but the $T\rightarrow(T+O_I)\rightarrow(O_I+O_{II})$ state change needed the sample cooling. Our experimental data in Figs. 5 and 6 were, in fact, obtained after the sample was kept at each temperature for about 1 hr. Further, the strain relaxation may occur in the thin samples for TEM observation. These factors should be taken into account in formulating a better understanding of the unique evolution of the domain structures during the T-to-O transition. Although the thermal path experienced by a sample plays a crucial role in the domain-structure evolution, the coupling between the JT and O distortions is most probably the main origin of the unique behavior found in this transition.

V. CONCLUSIONS

Our low-temperature *in situ* observation using the transmission electron microscope revealed that in $Sr_{2-x}La_xMnO_4$ the O phase present in the $0.10\leqslant x\leqslant 0.20$ composition region was identified as the FD state characterized by orbital ordering without charge ordering. The microstructure of the O phase was found to consist of two O variants with different b/a values, not the usual twin structure of two variants having the same b/a value. The most interesting phenomena observed is that the evolution of these two O variants during the T-to-O phase transition occurs in three steps: the appearance of the $(T+O_I)$ and then (O_I+O_{II}) microstructures, followed by the annihilation of some O_I and O_{II} regions at lower temperatures in the O phase. Because the $(T+O)$ and (O_I+O_{II}) microstructures can be regarded as two modulation modes for the strain modulation, the domain-structure evolution during the T-to-O phase transition seems to have some similarity to the phenomenon occurring in the spinodal decomposition for the modulation of chemical composition. But the presence of these microstructures is obviously the distinct characteristic of this strain modulation, resulting from the coupling between the JT and O distortions, the importance of which was recently pointed out by Ahn and coworkers.[6–9]

[1] S. Jin, T. H. Tiefel, M. McCormack, R. A. Fastnacht, R. Ramesh, and L. H. Chen, Science **264**, 413 (1994).
[2] Y. Tokura, A. Urushibara, Y. Moritomo, T. Arima, A. Asamitsu, G. Kido, and N. Furukawa, J. Phys. Soc. Jpn. **63**, 3931 (1994).
[3] G. C. Xiong, Q. Li, H. L. Ju, S. N. Mao, L. Senapati, X. X. Xi, R. L. Greene, and T. Venkatesan, Appl. Phys. Lett. **66**, 1427 (1995).
[4] Y. Tokura and N. Nagaosa, Science **288**, 462 (2000).
[5] E. Dagotto, T. Hotta, and A. Moreo, Phys. Rep. **344**, 1 (2001).
[6] K. H. Ahn, T. Lookman, and A. R. Bishop, Nature (London) **428**, 401 (2004).
[7] K. H. Ahn, T. Lookman, A. Saxena, and A. R. Bishop, Phys. Rev. B **68**, 092101 (2003).
[8] K. H. Ahn, T. Lookman, A. Saxena, and A. R. Bishop, Phys. Rev. B **71**, 212102 (2005).
[9] T. Lookman, S. R. Shenoy, K. O. Rasmussen, A. Saxena, and A. R. Bishop, Phys. Rev. B **67**, 024114 (2003).
[10] J. Burgy, M. Mayr, V. Martin-Mayor, A. Moreo, and E. Dagotto, Phys. Rev. Lett. **87**, 277202 (2001).
[11] E. Dagotto and A. Moreo, J. Magn. Magn. Mater. **226**, 763 (2001).
[12] P. Bak and J. vonBoehm, Phys. Rev. B **21**, 5297 (1980).
[13] P. Bak, Rep. Prog. Phys. **45**, 587 (1982).
[14] Y. Yamada and T. Takakura, J. Phys. Soc. Jpn. **71**, 2480 (2002).
[15] Y. Moritomo, Y. Tomioka, A. Asamitsu, Y. Tokura, and Y. Matsui, Phys. Rev. B **51**, 3297 (1995).
[16] Y. Moritomo, A. Nakamura, S. Mori, N. Yamamoto, K. Ohoyama, and M. Ohashi, Phys. Rev. B **56**, 14879 (1997).
[17] W. Bao, C. H. Chen, S. A. Carter, and S.-W. Cheong, Solid State Commun. **98**, 55 (1996).
[18] S. Larochelle, A. Mehta, N. Kaneko, P. K. Mang, A. F. Panchula, L. Zhou, J. Arthur, and M. Greven, Phys. Rev. Lett. **87**, 095502 (2001).
[19] S. Larochelle, A. Mehta, L. Lu, P. K. Mang, O. P. Vajk, N. Kaneko, J. W. Lynn, L. Zhou, and M. Greven, Phys. Rev. B **71**, 024435 (2005).
[20] T. Kimura, K. Hatsuda, Y. Ueno, R. Kajimoto, H. Mochizuki, H. Yoshizawa, T. Nagai, Y. Matsui, A. Yamazaki, and Y. Tokura, Phys. Rev. B **65**, 020407(R) (2001).
[21] T. Nagai, T. Kimura, A. Yamazaki, T. Asaka, K. Kimoto, Y. Tokura, and Y. Matsui, Phys. Rev. B **65**, 060405(R) (2002).
[22] M. Daghofer, A. M. Oles, D. R. Neuber, and W. Linden, Phys. Rev. B **73**, 104451 (2006).
[23] J. Tao, D. Niebieskikwiat, M. B. Salamon, and J. M. Zuo, Phys. Rev. Lett. **94**, 147206 (2005).
[24] T. Miyazaki, S. Takagishi, H. Mori, and T. Kozakai, Acta Metall. **28**, 1143 (1980).
[25] Y. Koyama, Acta Metall. Mater. **38**, 857 (1990).